

Rough-Surface-Enabled Capacitive Pressure Sensors with 3D Touch Capability

Kilsoo Lee, Jaehong Lee, Gwangmook Kim, Youngjae Kim, Subin Kang, Sungjun Cho, SeulGee Kim, Jae-Kang Kim, Wooyoung Lee, Dae-Eun Kim, Shinill Kang, DaeEun Kim, Taeyoon Lee,* and Wooyoung Shim*

Fabrication strategies that pursue “simplicity” for the production process and “functionality” for a device, in general, are mutually exclusive. Therefore, strategies that are less expensive, less equipment-intensive, and consequently, more accessible to researchers for the realization of omnipresent electronics are required. Here, this study presents a conceptually different approach that utilizes the inartificial design of the surface roughness of paper to realize a capacitive pressure sensor with high performance compared with sensors produced using costly microfabrication processes. This study utilizes a writing activity with a pencil and paper, which enables the construction of a fundamental capacitor that can be used as a flexible capacitive pressure sensor with high pressure sensitivity and short response time and that it can be inexpensively fabricated over large areas. Furthermore, the paper-based pressure sensors are integrated into a fully functional 3D touch-pad device, which is a step toward the realization of omnipresent electronics.

In recent years, considerable interest in flexible electronics has resulted in numerous efforts toward evolving these devices into more advanced forms such as flexible displays,^[1,2] diagnostic devices,^[3,4] electronic skins,^[5–7] and energy-harvesting devices.^[8,9] Paper is considered a promising flexible substrate for the realization of such advanced flexible electronics because of its excellent flexibility, low cost, disposability, light weight, and biodegradability. The use

of paper substrates has thus been intensively investigated for the fabrication of various paper-based flexible electronic components, including displays,^[10,11] touch pads,^[12] microfluidic devices,^[13–16] supercapacitors,^[17–21] transistors,^[22] and sensors.^[23–27] The development of appropriate printing techniques for paper-based electronics, such as dip-coating, spin-coating, sputtering, evaporation, inkjet printing, and writing techniques, has also been widely investigated.^[28–37] Among these methods, the pen-on-paper (PoP) approach using a pencil offers a unique low-cost and simple method for depositing conducting graphite electrodes and fabricating paper-based flexible devices using a drawing process.^[35–37] Even though the fabrication of paper-based electronic devices with high functionality is difficult using this technique because of the resulting rough surface, which hinders the achievement of high electrical conductance,^[29,35] the PoP approach provides a simple and efficient method of depositing conductive electrodes on paper.

Among paper-based electronic devices, flexible pressure sensors have been widely investigated because of their potential application for wearable skins,^[34,38] diagnostics,^[38] microelectromechanical system sensors,^[39] and human motion detection.^[34,38–44] Microstructured capacitive pressure sensors, which use compressible microstructural deformations and an effective increase of the dielectric constant,

K. Lee, G. Kim, Y. Kim, S. Cho,
Prof. W. Lee, Prof. W. Shim
Department of Materials Science and Engineering
Yonsei University
50 Yonsei-ro, Seodaemun-Gu
Seoul 03722, Republic of Korea
E-mail: wshim@yonsei.ac.kr

Dr. J. Lee, S. Kang, S. Kim, Prof. D. Kim, Prof. T. Lee
School of Electrical and Electronic Engineering
Yonsei University
50 Yonsei-ro, Seodaemun-Gu, Seoul 03722, Republic of Korea
E-mail: taeyoon.lee@yonsei.ac.kr

J.-K. Kim, Prof. D.-E. Kim, Prof. S. Kang
School of Mechanical Engineering
Yonsei University
50 Yonsei-ro, Seodaemun-Gu, Seoul 03722, Republic of Korea

DOI: 10.1002/sml.201700368



have been developed for use as high-performance flexible pressure sensors with sensitive responses to external stimulation.^[3,45–51] Various fabrication techniques have been established for these devices, which can be categorized as (i) synthetic approaches, in which elastomeric foams that contain entrapped air enhance the compressibility and sensitivity;^[45–51] (ii) lithographic approaches, in which microfabricated pyramidal or porous structures enhance the response and relaxation time as well as sensitivity;^[45–49] or (iii) hybrid approaches, in which active devices such as transistors are interfaced with the microstructured elastomer as gate dielectrics, resulting in high sensor performance because of the superlinear characteristics of the transistor.^[3,45] To this end, we recently introduced microstructured resistive pressure sensors and demonstrated their reflective-type color display upon pressure loading through modulation of the resistance in a pyramidal electrical switch.^[7] The microstructured sensor represents a significant advance in that it eliminates most of the drawbacks of the incompressible and viscoelastic nature of bulk rubbers and controls the effective dielectric constant using the volumetric change of the airgap to maximize the sensitivity. This approach, however, does not offer a less equipment-intensive process than that afforded by simple paper-based fabrication. To achieve facile fabrication (simplicity) that does not compromise the pressure sensitivity (functionality), a novel approach capable of mimicking microstructured dielectric surfaces must be developed that does not rely on microfabrication processes.

Here, we present a conceptually different approach that utilizes the inartificial design of the surface roughness of paper to realize a capacitive pressure sensor with high performance compared with sensors produced using costly

microfabrication processes. We view the “rough surface” of the paper as microstructures, enabling an increase of the effective dielectric constant that can enhance the pressure sensitivity upon loading. We demonstrate that these paper-based capacitive pressure sensors can exhibit pressure sensitivity (0.62 kPa^{-1}), short response and relaxation times (on the order of hundreds of milliseconds), a low limit of detection (6 Pa), high stability under repeated loading (5000 cycles), and excellent bending stability (1000 cycles). Furthermore, we demonstrate that the integration of these pressure sensor elements into an array readily yields a functional force-touch device that is capable of acting as a pressure sensor-based peripheral input device, which is a step toward the realization of advanced paper electronics that combine high simplicity and functionality.

The key innovation that enables the development of a paper-based capacitive pressure sensor is a new protocol for utilizing the microstructure-like randomly rough surface of graphite-coated paper, which allows the formation of an airgap when two graphite-coated papers face each other (Figure 1a). This concept enables the fabrication of devices that are comparable to those produced using costly microfabrication processes (Figure S1, Supporting Information). To fabricate the paper-based pressure sensor, a pencil (8B) was used to transfer graphite onto paper (Figure 1b). The roughness (R_c , mean height of the profile elements) of the paper was $\approx 10 \mu\text{m}$, and that of the graphite electrode on the paper was smaller ($\approx 7 \mu\text{m}$) because of the contact pressure during writing (Figure S2, Supporting Information). The average sheet resistance of the transferred graphite electrode was $800 \Omega/\text{sq}$. Next, to fabricate the capacitive pressure sensor, a polydimethylsiloxane (PDMS) film was coated onto the

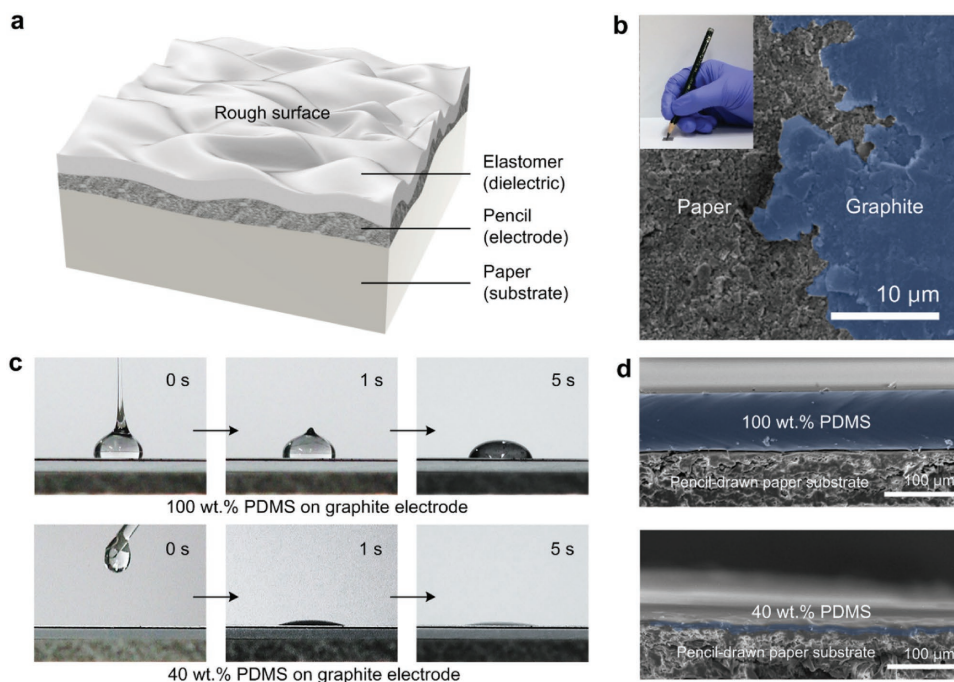


Figure 1. a) Schematic illustration of the microstructure-like randomly rough surface. b) SEM image of the graphite (blue) on the paper. The inset shows a photograph of the writing process on the paper using an 8B pencil. c) Consecutive photographs of liquid droplets of 100 wt% PDMS (top) and 40 wt% PDMS (bottom) dropped on the graphite-coated paper with time intervals of 0, 1, and 5 s. d) Cross-sectional view of SEM images of the 100 wt% PDMS (top) and 40 wt% PDMS (bottom) coated on the graphite-electrode-drawn paper.

graphite electrodes on papers using a PDMS solution diluted with heptane. The film was sufficiently thin that the roughness of the graphite electrodes was maintained. The dissolution of PDMS in a solvent depends on the solubility parameter (δ) defined by the Hildebrand–Scatchard equation. A solvent with a δ value similar to that of PDMS can dissolve PDMS effectively because the free energy of mixing is favorable.^[52] The δ values for heptane and PDMS are 7.4 and 7.3 cal^{1/2} cm^{-3/2}, respectively, thereby justifying the selection of heptane as a solvent.^[52] Compared with the 100 wt% PDMS solution (viscosity: ≈ 3.52 Pa s), the PDMS solution diluted with heptane (40 wt% PDMS) exhibited a liquid-like low viscosity (≈ 0.02 Pa s), as shown in Figure 1c.^[53] Importantly, when spin-coated at 1000 rpm for 30 s, the 40 wt% PDMS solution formed a 6 μ m thick film with a surface roughness comparable to that of the graphite electrode, thereby preserving its rough geometry (4 μ m). This behavior contrasts with that of the 100 μ m thick film of the 100 wt% PDMS solution, which flattened the surface with a roughness of 600 nm (Figure S3, Supporting Information). This finding indicates that the 40 wt% PDMS conformably coated the rough surface of the graphite-covered paper such that the roughness was preserved (Figure 1d). In addition, we confirmed the good adhesion between the 40 wt% PDMS and graphite electrode on the paper for up to 100 cycles through bending tests, as shown in Figure S4 in the Supporting Information.

We constructed a single-cell capacitor in which the half-cell consisted of a graphite electrode on paper coated with a layer of PDMS dielectric; another identical half-cell capacitor was then sequentially placed to yield a metal–insulator–metal sandwich structure (Figure 2a). Figure 2b presents a representative photograph of the fabricated pressure sensor. Briefly, a 4 \times 2 cm² piece of a 120 μ m thick sheet of paper (PAX laser printer paper) patterned using a graphite pencil was placed onto the glass slide and spin-coated with 40 wt% PDMS diluted with heptane. Following the curing of PDMS, gold textile electrical leads (Solueta Co. Ltd. SILTEX, CNG type) were wired in series between the graphite electrodes and voltage source, and then, two half-cells were overlapped to complete the capacitor (Figure 2b). In this manner, we fabricated and tested capacitor elements with sizes of 1 \times 1 cm² for two graphite electrodes, where the pristine roughness of the graphite electrode was still preserved and could be utilized to increase the capacitive response of the pressure sensor under pressure (Figure 2c). Capacitance analysis with time for seven cycles of applied pressures of 0.5, 1, 2, and 5 kPa revealed that this fabrication protocol did indeed yield a pressure sensor (Figure 2d). Reliable and repeatable sensing behavior was observed; the capacitance of the sensor changed sharply with pressure loading and unloading. The estimated response and recovery times upon loading (5 kPa) and unloading, defined as time constants given by

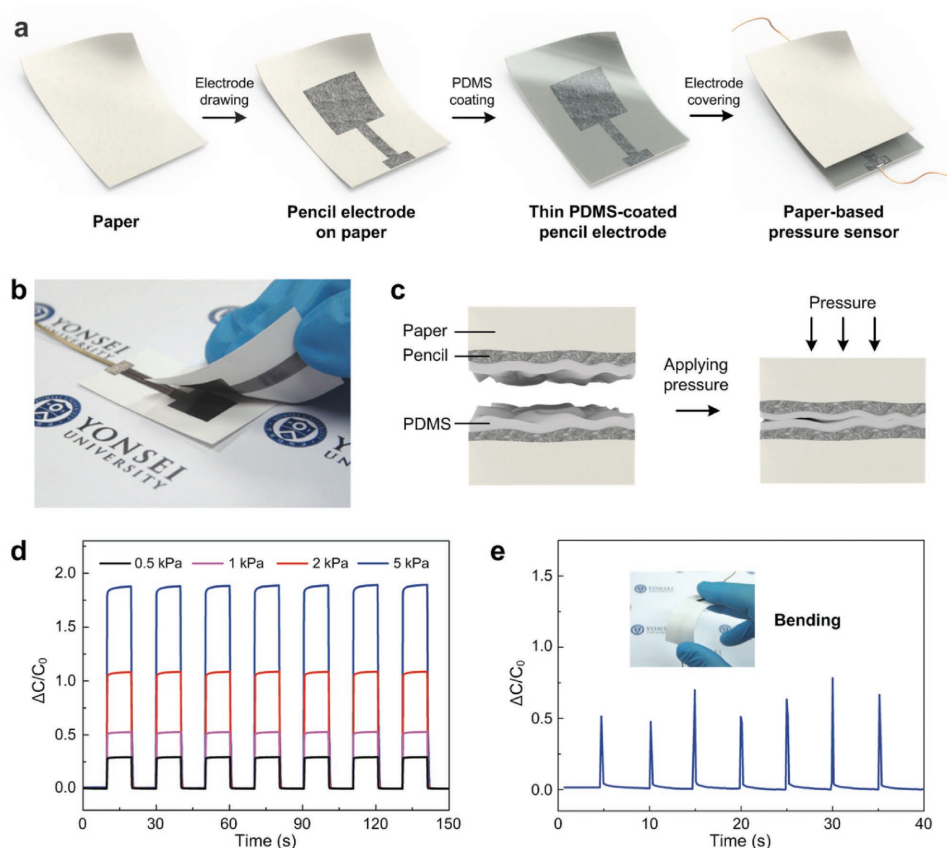


Figure 2. a) Schematic process for the fabrication of the paper-based capacitive pressure sensor. b) Photograph of the fabricated pressure sensor. c) Schematic depiction of the pressure sensor under applied pressure. d) Capacitive response as a function of time under repeated normal pressure loading-unloading cycles of 0.5, 1, 2, and 5 kPa. e) Instantaneous capacitive response to dynamic loading-unloading cycles of bending.

1 - 1/e ($\approx 63\%$) (for response) and 1/e ($\approx 36\%$) (for recovery), were on the order of milliseconds. Note that the baseline capacitance of the capacitor with the 40 wt% PDMS dielectric ($6 \mu\text{m}$ thick) was $\approx 30 \text{ pF cm}^{-2}$, minimizing the effect of parasitic capacitance and increasing the signal-to-noise ratio compared with that of the 100 wt% PDMS dielectric (baseline capacitance: 18 pF cm^{-2}). In addition, the paper substrate was reversibly flexible, enabling the use of bending tests for evaluation of the tangential pressure-sensing ability; the resulting sensor performance offered a reasonable instantaneous 50% capacitance change (Figure 2e). The capacitance change of the sensor as a function of bending radius was also evaluated (Figure S5, Supporting Information). Finally, the sensor exhibited excellent stability against repeated bending tests for 1000 cycles (Figure S6, Supporting Information).

Next, the pressure-sensing capabilities of the paper-based capacitive pressure sensor—including the ability to control the effective dielectric constant and the areas of the electrodes—were evaluated by measuring changes in the capacitance and electrical conductance, respectively. The sensitivities of the capacitive pressure sensors were measured under the application of normal pressure (0–80 kPa); the sensitivity was defined as $S = \delta(\Delta C/C_0)/\delta p$, where p is the normal pressure and C and C_0 are the capacitances with and without normal pressure, respectively (Figure 3a; Figure S7 in the Supporting Information). Upon normal-pressure loading, a distance between electrodes, d , decreased and thus C increased in the general pressure sensor using the elastomeric dielectric layer.

Initially, S of the 100 wt% PDMS-coated paper-based capacitive pressure sensor, whose surface was flat (as observed in Figure 1c), was measured to be 0.004 kPa^{-1} in the 0–11 kPa range (Figure 3a). In contrast, S of the 40 wt% PDMS-coated paper-based capacitive pressure sensor was 0.62 kPa^{-1} for pressures below 2 kPa (Figure 3a), which is comparable to the sensitivities of sophisticated microfabricated pressure sensors.^[45–49] In addition, we evaluated the sensitivities of various capacitive pressure sensors fabricated on different types of paper using identical PDMS conditions (Figure S8, Supporting Information). The pressure sensitivities differed slightly depending on the roughness and curl of the paper. However, overall, the pressure sensors consisting of 40 wt% PDMS coated on different types of paper exhibited higher sensitivities than those using 100 wt% PDMS-coated paper.

Qualitatively, several factors contribute to the high sensitivities of our paper-based capacitive pressure sensors. First, the 40 wt% PDMS-coated surface has a surface curl, which leads to the formation of a large-volume airgap between the two PDMS/graphite/paper sheets when they face each other (Figure S9 and Movie S1, Supporting Information). Similar to the surface curl of a layered structure, that of the paper-based pressure sensors develops under a small compressive strain^[54] produced during writing for the graphite/paper and curing for the PDMS/graphite/paper (Figure S10, Supporting Information). This airgap enables the distance d to be changed even under low pressures based on the high flexibility of the paper, resulting in a large change of the capacitance and,

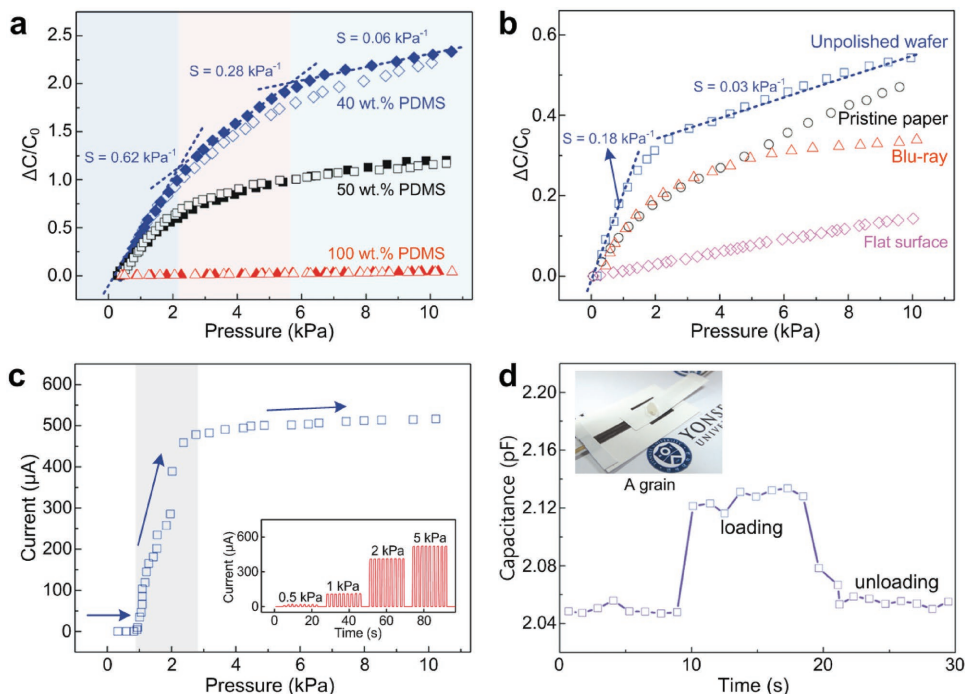


Figure 3. a) Capacitive response as a function of pressure for different concentrations of PDMS in heptane (40 wt% (blue), 50 wt% (black), 100 wt% (red)). b) Effect of rough-surface-molded PDMS on the capacitive pressure response. Unpolished silicon wafer- (blue), pristine paper- (black), and blu-ray-molded PDMS (red) were prepared on flat ITO electrodes (Figure S12, Supporting Information). c) Electrical current as a function of pressure at incrementally increasing pressure for the interlocked graphite electrodes. The pressure induces an increase in the contact area between the interlocked graphite, which causes an increase in the electrical current. The inset shows the electrical current as a function of time under repeated normal pressure values of 0.5, 1, 2, and 5 kPa. d) Response of the paper-based capacitive pressure sensor to the loading and removal of a small weight (a grain of rice, weight: 8 mg, corresponding to a pressure of 6 Pa).

consequently, sensitivity. Second, the 40 wt% PDMS film conformably coats the rough surface of the graphite-covered paper such that the roughness is preserved (Figure S11, Supporting Information). This roughness enables the formation of a small airgap in an equivalent manner as a microstructured periodic surface or porous PDMS,^[45–50] allowing sensitive response in the low-pressure region. In a series of experiments in which unpolished silicon wafer- ($R_c \approx 2 \mu\text{m}$), pristine paper- ($R_c \approx 800 \text{ nm}$), and blu-ray ($R_c \approx 70 \text{ nm}$)-molded rough PDMS surfaces were prepared on flat indium tin oxide (ITO) electrodes (Figure S12, Supporting Information) to clarify the effect of the rough surface of the PDMS layer on the sensitivity, the resulting sensitivities of 0.18, 0.10, and 0.10 kPa^{-1} , respectively, were indeed higher than that of the 100 wt% flat PDMS (Figure 3b). Even higher sensitivity was attained with a rougher surface; however, the roughness itself does not contribute to the high sensitivity. Instead, the combined effect of large and small airgaps created by the surface curl and surface roughness contributes to the high sensitivity of the pressure sensor. The external pressure reduces the large and small airgaps ($\epsilon \approx 1.0$), thereby leading to increases in the effective dielectric constant and pressure sensitivity. Third, for the electrode, randomly rough graphite surfaces are interlocked upon loading, increasing the overlapped electrode areas of the capacitive pressure sensor (Figure S13, Supporting Information). To quantify the effect of this interlocked geometry, the relative electrical currents ($\Delta I/I_0$) of two graphite electrodes facing each other without a PDMS layer were measured for different pressures (Figure 3c). The electrical current increased with increasing pressure with (i) a slight change below 1 kPa ($\approx 10 \mu\text{A}$), (ii) an abrupt change between 1 and 3 kPa ($\approx 480 \mu\text{A}$), and (iii) a gradual change above 3 kPa ($\approx 510 \mu\text{A}$). The increase in electrical current can be primarily attributed to the increased overlap of the interlocked graphite bumps and, consequently, the contact area (Figure S13, Supporting Information). In a simple contact mechanics model,^[55] the contact area of a rough surface consists of spherical bumps of equal radius of curvature but with a Gaussian distribution of heights that is nearly proportional to the pressure, $A \propto F^{2/3}$, which is in reasonably good agreement with the observed results. The ability to control the effective dielectric constant with decreasing distance and, in particular, to increase the contact area makes this approach distinct from those presented in previous studies and can provide high sensitivity. Note that the pressure sensor sensitivities do not depend on the original thickness of the PDMS film but on the surface curl and roughness of the pressure sensor (Figure S14, Supporting Information). Figure 3d presents an explicit demonstration of this ultrasmall weight sensing using a grain of rice (8 mg), which corresponds to a pressure of only 6 Pa.

By taking advantage of the porous fiber scaffold of the paper, it is possible to enhance the relaxation property of the capacitive pressure sensor. **Figure 4a** and Figure S15 (Supporting Information) show the response and relaxation times of the pressure sensors fabricated using 100 wt% (100 μm thick) and 40 wt% PDMS (6 μm thick) upon the loading (5 kPa) and unloading of the sensor. The response times to the load differed slightly for the two pressure sensors (1 s and

200 ms for the 100 wt% and 40 wt% PDMS sensors, respectively), whereas significant differences were observed for the relaxation times (over 10 s and less than 1 s (e.g., 400 ms) for the 100 wt% and 40 wt% PDMS sensors, respectively). Given that the 40 wt% PDMS film (6 μm) was much thinner than the paper (120 μm), the properties of the paper, whose behavior was nearly elastic under the applied loading and unloading conditions, could play a dominant role. To further examine this idea, cyclic loading–unloading experiments, in the context of a compressive stress–strain curve, were performed on pristine paper without the PDMS film (Figure 4b). A set of 100 individual loading–unloading cycles with a maximum load of 0.1 N ($\approx 10 \text{ kPa}$) were performed. Hysteresis was observed between the loading and unloading paths in the first loading–unloading cycle (gray curve); in addition, a residual displacement of 3.5 μm was observed after the loading–unloading cycle, which implies that some permanent deformation, possibly plastic flow of the fiber, occurred. However, after the first loading–unloading cycle, the loading data in each cycle were characterized by elastic loading followed by a linear response; application of the load corresponded to moving from the origin up and along a straight line, and upon release of the load, the line traversed in the opposite direction back to the origin. The observed elasticity in the loading–unloading cycles can likely be attributed to the curled nature of the paper (Figure S9, Supporting Information), which implies that elasticity was a structural response rather than a material one.

Based on the observed results, we modeled the effect of elasticity of the 40 wt% PDMS film and paper substrate. First, the Kelvin–Voigt model^[56] (an empirical model for a viscoelastic solid consisting of a spring and dashpot connected in a parallel arrangement) was adopted to describe the viscoelasticity of the PDMS films. This model adequately accounts for the behavior of a viscoelastic solid but not a viscoelastic liquid, which is described by the Maxwell model, in which the spring and dashpot are connected in series. For the paper/PDMS structure, we combined two Kelvin–Voigt models in series, as PDMS is a well-known viscoelastic material and the paper itself exhibited viscoelastic behavior.^[57–59] Second, according to Figure 4b, the curly paper substrate that formed the airgap was assumed to be elastic and, thus, equivalent to a spring. Third, combining the spring model (curly paper substrate) with two Kelvin–Voigt models (paper/PDMS film), we constructed a viscoelastic model composed of a spring and Kelvin–Voigt solid connected in series (Figure 4c), which is similar to the standard viscoelastic solid model.^[56] The material function relating the stress, strain, and strain rate for this model can be expressed as

$$\sigma_{\text{total}} = \frac{1}{3} \cdot (\sigma_{\text{paper curl}} + \sigma_{\text{PDMS}} + \sigma_{\text{paper}}) = \frac{1}{3} \cdot \left\{ (E_{\text{paper curl}} \cdot \epsilon_{\text{paper curl}}) + \left(E_{\text{PDMS}} \cdot \epsilon_{\text{PDMS}} + \eta_{\text{PDMS}} \frac{d\epsilon_{\text{PDMS}}}{dt} \right) + \left(E_{\text{paper}} \cdot \epsilon_{\text{paper}} + \eta_{\text{paper}} \frac{d\epsilon_{\text{paper}}}{dt} \right) \right\},$$

where σ is the normal stress, ϵ is the normal strain, $\frac{d\epsilon}{dt}$ is the strain rate, E is the elastic modulus, and η is the viscosity coefficient of the material. Because our measured $E_{\text{paper curl}}$ ($\approx 30 \text{ kPa}$) is 30 times smaller than E_{PDMS} ($\approx 1 \text{ MPa}$),^[60] when the stress σ_{total} is applied, most

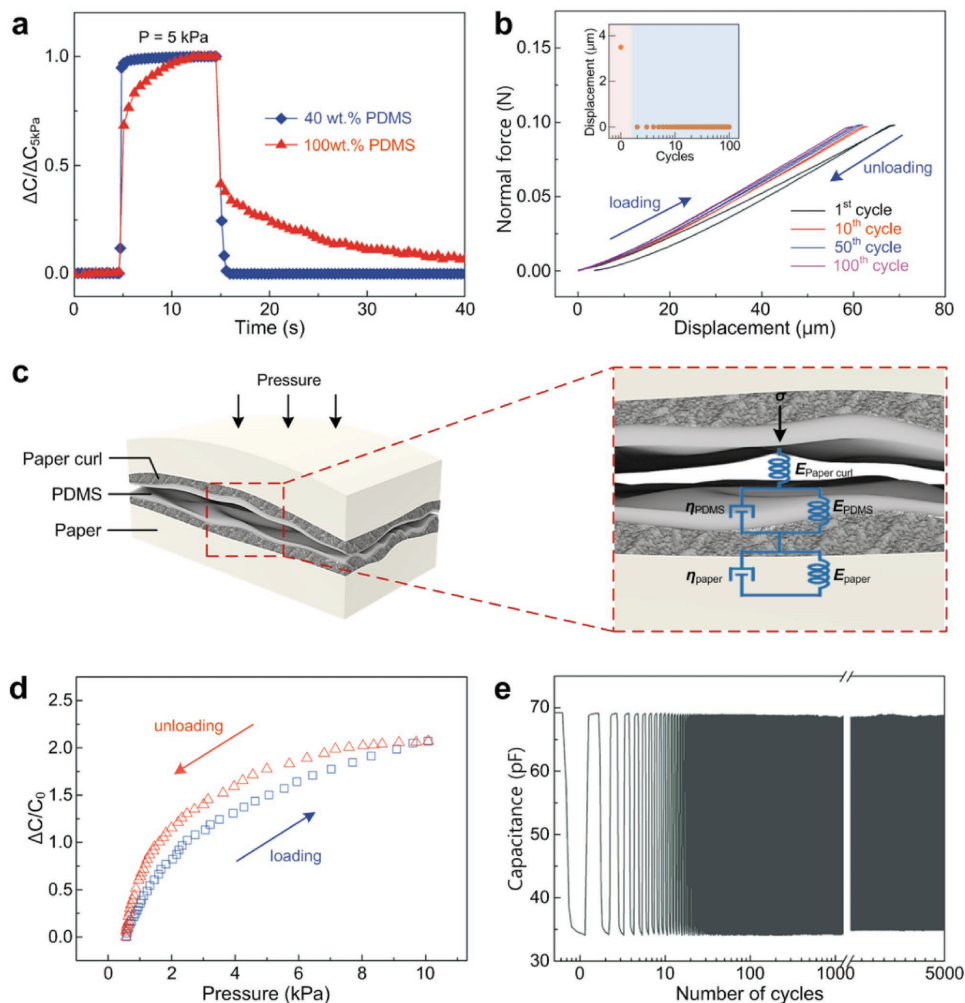


Figure 4. a) Comparison of response and relaxation times between 40 wt% PDMS- and 100 wt% PDMS-coated pressure sensors after loading (5 kPa for 10 s) and unloading. b) Repeated normal force–displacement curves using nanoindentation measurement on pristine paper, showing the elastic property of the curly paper. The inset shows the curly paper after the first loading–unloading cycle. c) Schematic illustration of the model consisting of a spring model (curly paper substrate) and two Kelvin–Voigt models (paper/PDMS film) connected in series. d) Relative capacitance change from two consecutive linear loading (10 kPa) and unloading cycles for 40 wt% PDMS-coated capacitive pressure sensor. e) Stability of capacitive response of the 40 wt% PDMS-coated capacitive pressure sensor to a load of 2 kPa over 5000 cycles.

deformation occurs in the paper curl, indicating less compression in the viscoelastic PDMS and, consequently, increased system elasticity. Given that $E_{\text{paper}} (\approx 20 \text{ MPa})$ ^[58,61] is much larger than E_{PDMS} , compression in the paper itself is highly unlikely, thereby validating our models for the (i) 100 wt% PDMS/paper (Figure S16 for quantitative analysis, Supporting Information), where the PDMS is the dominant factor, and (ii) 40 wt% PDMS/paper curl, where the paper curl is the dominant factor. Because the relaxation property of the paper-based pressure sensor with 40 wt% PDMS film is mainly determined by the paper curl, the relaxation times are not related to the thickness of the PDMS films, as shown in Figure S17 (Supporting Information). In this regard, two characteristics—stability and robustness—were characterized on a $1 \times 1 \text{ cm}^2$ pressure sensor. In the former case, the hysteresis, which is the consecutive linear loading–unloading cycle up to 10 kPa in the context of the pressure response curves (Figure 4d), was small, providing the 40 wt% PDMS/paper curl with structural elasticity. In the latter case, the sensor

endured 5000 loading–unloading cycles with 2 kPa and maintained its full function with minimal output signal degradation (Figure 4e).

The force-sensing capability of the paper-based capacitive pressure sensor is distinguished from that of all other pressure sensors. Distinctive sensitivity levels can be built with the sensor responding differently to variation in pressure, and an integrated sensor array can be formed over a full-size sheet of paper ($210 \times 297 \text{ mm}^2$, A4 size) to create 3D input devices. 3D input devices can perceive the magnitude of normal force applied on the device. As a proof-of-concept experiment, the capacitance change of a 3×3 multiple-pixel pressure sensor array, where the area of each pixel was $1 \times 1 \text{ cm}^2$ and the spacing between pixels was 1.3 cm, was evaluated. Bearing balls with weights of 5 or 50 g were placed in each pixel; these weights corresponded to pressures of ≈ 0.5 and 5 kPa, respectively (Figure 5a). The corresponding capacitive response of the array is shown in Figure 5b: the spatial distribution ((1,1) and (2,3) in x – y coordinates, respectively) and resolution

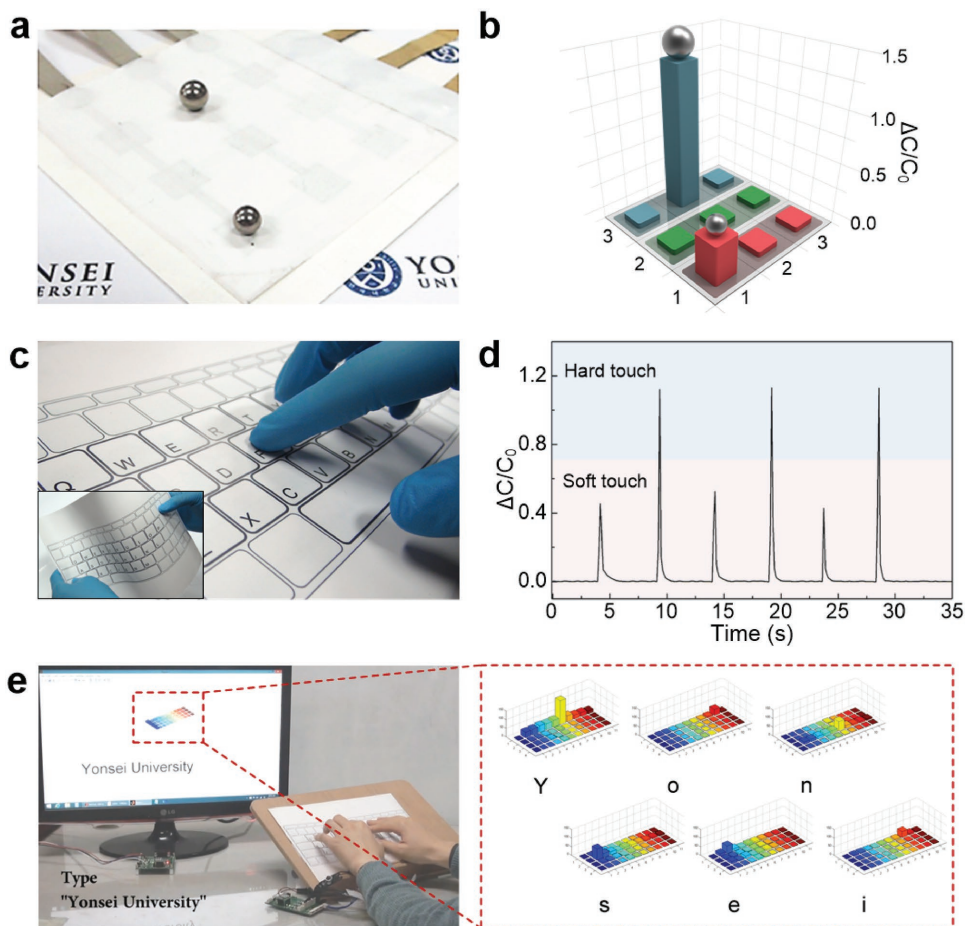


Figure 5. a) Photograph of the 3×3 multiple-pixel pressure sensor array. b) Reconstructed map with column heights corresponding to the relative capacitance changes (two bearing balls of 5 and 50 g that correspond to pressure values of 0.5 and 5 kPa, respectively). c) Photograph showing paper keyboard composed of 27 pressure sensor keys including all the alphabet keys and a space bar. The photograph in the inset demonstrates the flexibility of the paper keyboard. d) Relative capacitive response of keys from the consecutive input combination (soft- and hard-finger touch). e) Photograph of typing “Yonsei University” using the paper keyboard (left). The magnitude of response for each letter of “Yonsei” is shown on the right, demonstrating that the device is capable of distinguishing uppercase and lowercase letters depending on the applied pressure.

(0.27 and 1.33 in $\Delta C/C_0$, respectively) from the external pressure can be successfully distinguished by the capacitive response of each pixel in the array.

Next, we demonstrated the potential of a full-size keyboard to realize a substantially functional pressure sensor. Figure 5c presents a photograph of the fabricated paper keyboard with 27 pressure sensors corresponding to the 26 alphabet keys and the space bar; the flexibility of the keyboard is also demonstrated (inset of Figure 5c). To minimize crosstalk in the keyboard, each pressure sensor was designed to be 0.8 cm in width with a spacing of 1.2 cm between each sensor (Figure S18, Supporting Information). Figure 5d presents representative input (finger-touch)/output (capacitive change) data for the consecutive input combination (soft- and hard-touch). The output of the different soft- and hard-touch combinations indicates that the $\Delta C/C_0$ values were distantly separated and had similar values for each key (0.4 for soft-touch and 1.2 for hard-touch), which is consistent with our results for the smaller 3×3 sensor array described above. This narrow distribution of the output for both soft-touch (0.4 in $\Delta C/C_0$) and hard-touch (1.2 in $\Delta C/C_0$) suggests that further-integrated 3D inputs are possible using

this approach. To demonstrate this concept, the keyboard was connected to a data-acquisition (DAQ) circuit for the read function of the capacitive responses and transmission of data to the computer (Figure S19, Supporting Information). The DAQ system efficiently collected the capacitive responses by measuring the discharging times of the stored charges in each capacitive pressure sensor (Figure S20, Supporting Information). The capacitive responses of each key against finger-touch were demonstrated by typing the letters. For example, the letters of “YONSEI UNIVERSITY” were typed and presented on a monitor screen in real time, as demonstrated in Movie S2 (Supporting Information). Furthermore, our pressure sensors, which could distinguish between the soft- and hard-touch intensities, could realize a 3D force touch that assigns multiple functions to a key. We could input both a lowercase and an uppercase letter using only one key based solely on the magnitude of the applied pressure. To distinguish between the soft- and hard-touch, a certain discharging time (0.7 ms) in the DAQ system was used as the threshold value. Indeed, as demonstrated in Figure 5e and Movie S3 (Supporting Information), the letters of “Yonsei University” were successfully inputted into the computer without using a

toggle key such as Caps Lock; the magnitude of the applied pressure used when touching each letter is shown in the inset of Figure 5e and accordingly determined whether the letter should be uppercase or lowercase. Although the paper keyboard (lightweight, portable, flexible, and paper-thin) is presented as the first example of this omnipresent strategy, one can envision even more functional applications of this capacitive pressure-sensing capability.

We have developed a new concept whereby the rough surface of paper can be inartificially utilized to enable realization of high-performance pressure sensors that have not been proposed in the context of surface roughness. Although most researchers on paper-based electronics to date have struggled to build both passive and active circuit elements using paper substrates because of the issue of microscale roughness, the use of this nature simply leads to highly functional sensing devices. We have also demonstrated that the elastic behavior of the paper is readily apparent and that the temporal response of the sensors is fast enough upon the application of pressure. This approach does have disadvantages compared with previously reported techniques. For example, it is limited by a low resolution in terms of width and registration of conducting electrodes, which thereby limits its scale-up potential. However, this constraint may be addressed by utilizing the ink-jet printing technique to increase the resolution and enable mass production. By providing approaches to address the (i) slow serial writing process, (ii) bending-sensitive property of sensors, and (iii) crosstalk between sensing arrays, this approach offers significant advantages over many previous techniques in terms of sensitivity, temporal resolution, stability, and decreased complexity. Importantly, the cost of the prototype sensor array is comparable to that of the pencil and paper method, and this approach can be implemented omnipresently.

Experimental Section

Fabrication of Paper-Based Pressure Sensor: Graphite electrodes with desired patterns were deposited on paper (Paper Culture, PAX Laser printer paper) using a simple pencil-drawing process (Faber-Castell, 8B). PDMS (Dow Corning, Sylgard 184; 20:1 ratio of base to cross-linker by mass) was diluted with heptane (Sigma-Aldrich, Chromasolv Plus, for HPLC, 99%) to prepare the 40 wt% PDMS solution. The graphite-electrode-drawn paper was spin-coated with the 40 wt% PDMS solution at 1000 rpm for 30 s. The half-cell (PDMS-coated paper) was cured on a hot plate at 90 °C for at least 3 h. Two half-cells were stacked facing each other, with the vertical alignment of graphite electrodes forming a capacitor.

Characterization: The surface morphologies were examined using field-emission scanning electron microscopy (FE-SEM; JEOL, JSM-7001F) and laser scanning confocal microscopy (Keyence, VK-X200K). The electrical current measurements used to show the change in the contact area between the two electrodes were conducted using a source meter (Keithley 2400 with 1 V). The mechanical properties of the paper were characterized using nanoindentation (CSM Instrument, Switzerland). Capacitance measurements were performed at 100 kHz with a 1 V AC signal

using an LCR meter (Agilent E4980A, Precision LCR Meter). The force applied to the paper pressure sensor was manipulated by a universal manipulator (Teraleader) with 0.01 N resolution.

Supporting Information

Supporting Information is available from the Wiley Online Library and from the author.

Acknowledgements

K.L. and J.L. contributed equally to this work. This work was supported by the Small Grant for Exploratory Research (SGER) (NRF-2014R1A1A2A16055867); the Priority Research Centers Program (2009-0093823) through the National Research Foundation (NRF) of Korea; Midcareer Researcher Program through NRF grant funded by the MEST (2014R1A2A2A09053061); Yonsei University Future-leading Research Initiative of 2015 (2016-22-0062); National Research Foundation (NRF) of Korea Grant funded by the Korean Government (ERC-2015R1A5A1037668).

Conflict of Interest

The authors declare no conflict of interest.

- [1] M. S. White, M. Kaltenbrunner, E. D. Głowacki, K. Gutnichenko, G. Kettlgruber, I. Graz, S. Aazou, C. Ulbricht, D. A. M. Egbe, M. C. Miron, Z. Major, M. C. Scharber, T. Sekitani, T. Someya, S. Bauer, N. S. Sariciftci, *Nat. Photonics* **2013**, *7*, 811.
- [2] C. Wang, D. Hwang, Z. Yu, K. Takei, J. Park, T. Chen, B. Ma, A. Javey, *Nat. Mater.* **2013**, *12*, 899.
- [3] G. Schwartz, B. C.-K. Tee, J. Mei, A. L. Appleton, D. H. Kim, H. Wang, Z. Bao, *Nat. Commun.* **2013**, *4*, 1859.
- [4] J. A. Rogers, T. Someya, Y. Huang, *Science* **2010**, *327*, 1603.
- [5] D.-H. Kim, N. Lu, R. Ma, Y.-S. Kim, R.-H. Kim, S. Wang, J. Wu, S. M. Won, H. Tao, A. Islam, K. J. Yu, T. Kim, R. Chowdhury, M. Ying, L. Xu, M. Li, H.-J. Chung, H. Keum, M. McCormick, P. Liu, Y.-W. Zhang, F. G. Omenetto, Y. Huang, T. Coleman, J. A. Rogers, *Science* **2011**, *333*, 838.
- [6] M. Kaltenbrunner, T. Sekitani, J. Reeder, T. Yokota, K. Kuribara, T. Tokuhara, M. Drack, R. Schwödiauer, I. Graz, S. Bauer-Gogonea, S. Bauer, T. Someya, *Nature* **2013**, *499*, 458.
- [7] G. Kim, S. Cho, K. Chang, W. S. Kim, H. Kang, S. Ryu, J. Myoung, J. Park, C. Park, W. Shim, *Adv. Mater.*, **2017**, *29*, 1606120.
- [8] J. Chun, N.-R. Kang, J.-Y. Kim, M.-S. Noh, C.-Y. Kang, D. Choi, S.-W. Kim, Z. Lin Wang, J. Min Baik, *Nano Energy* **2015**, *11*, 1.
- [9] G. Zhou, L. Li, C. Ma, S. Wang, Y. Shi, N. Koratkar, W. Ren, F. Li, H.-M. Cheng, *Nano Energy* **2015**, *11*, 356.
- [10] A. C. Siegel, S. T. Phillips, B. J. Wiley, G. M. Whitesides, *Lab Chip* **2009**, *9*, 2775.
- [11] D. Y. Kim, A. J. Steckl, *ACS Appl. Mater. Interfaces* **2010**, *2*, 3318.
- [12] A. D. Mazzeo, W. B. Kalb, L. Chan, M. G. Killian, J.-F. Bloch, B. A. Mazzeo, G. M. Whitesides, *Adv. Mater.* **2012**, *24*, 2850.
- [13] M. S. Bhambhani, B. Benson, C. Chai, G. Katsikis, A. Johri, M. Prakash, *Nat. Biomed. Eng.* **2017**, *1*, 1.

- [14] A. W. Martinez, S. T. Phillips, G. M. Whitesides, E. Carrilho, *Anal. Chem.* **2010**, *82*, 3.
- [15] A. W. Martinez, S. T. Phillips, M. J. Butte, G. M. Whitesides, *Angew. Chem. Int. Ed.* **2007**, *46*, 1318.
- [16] M. M. Hamed, A. Ainla, F. Güder, D. C. Christodouleas, M. T. Fernández-Abedul, G. M. Whitesides, *Adv. Mater.* **2016**, *28*, 5054.
- [17] G. Zheng, L. Hu, H. Wu, X. Xie, Y. Cui, *Energy Environ. Sci.* **2011**, *4*, 3368.
- [18] Y. Wang, H. Zhou, *Energy Environ. Sci.* **2011**, *4*, 1704.
- [19] B. Yao, L. Yuan, X. Xiao, J. Zhang, Y. Qi, J. Zhou, J. Zhou, B. Hu, W. Chen, *Nano Energy* **2013**, *2*, 1071.
- [20] K.-H. Choi, J. Yoo, C. K. Lee, S.-Y. Lee, *Energy Environ. Sci.* **2016**, *9*, 2812.
- [21] G. Zheng, Y. Cui, E. Karabulut, L. Wågberg, H. Zhu, L. Hu, *MRS Bull.* **2013**, *38*, 320.
- [22] J. Huang, H. Zhu, Y. Chen, C. Preston, K. Rohrbach, J. Cumings, L. Hu, *ACS Nano* **2013**, *7*, 2106.
- [23] C.-W. Lin, Z. Zhao, J. Kim, J. Huang, *Sci. Rep.* **2014**, *4*, 3812.
- [24] X. Liao, Q. Liao, X. Yan, Q. Liang, H. Si, M. Li, H. Wu, S. Cao, Y. Zhang, *Adv. Funct. Mater.* **2015**, *25*, 2395.
- [25] P.-K. Yang, Z.-H. Lin, K. C. Pradel, L. Lin, X. Li, X. Wen, J.-H. He, Z. L. Wang, *ACS Nano* **2015**, *9*, 901.
- [26] K. A. Mirica, J. G. Weis, J. M. Schnorr, B. Esser, T. M. Swager, *Angew. Chem. Int. Ed.* **2012**, *51*, 10740.
- [27] F. Güder, A. Ainla, J. Redston, B. Mosadegh, A. Glavan, T. J. Martin, G. M. Whitesides, *Angew. Chem. Int. Ed.* **2016**, *55*, 5727.
- [28] D.-H. Kim, Y.-S. Kim, J. Wu, Z. Liu, J. Song, H.-S. Kim, Y. Y. Huang, K.-C. Hwang, J. A. Rogers, *Adv. Mater.* **2009**, *21*, 3703.
- [29] A. C. Siegel, S. T. Phillips, M. D. Dickey, N. Lu, Z. Suo, G. M. Whitesides, *Adv. Funct. Mater.* **2010**, *20*, 28.
- [30] Y. Zheng, Z. He, Y. Gao, J. Liu, *Sci. Rep.* **2013**, *3*, 1786.
- [31] A. Russo, B. Y. Ahn, J. J. Adams, E. B. Duoss, J. T. Bernhard, J. A. Lewis, *Adv. Mater.* **2011**, *23*, 3426.
- [32] D. Tobjörk, R. Österbacka, *Adv. Mater.* **2011**, *23*, 1935.
- [33] H. Liu, H. Qing, Z. Li, Y. L. Han, M. Lin, H. Yang, A. Li, T. J. Lu, F. Li, F. Xu, *Mater. Sci. Eng., R* **2017**, *112*, 1.
- [34] J. M. Nassar, M. D. Cordero, A. T. Kutbee, M. A. Karimi, G. A. T. Sevilla, A. M. Hussain, A. Shamim, M. M. Hussain, *Adv. Mater. Technol.* **2016**, *1*, 1600004.
- [35] N. Kurra, G. U. Kulkarni, *Lab Chip* **2013**, *13*, 2866.
- [36] Z. Li, H. Liu, C. Ouyang, W. H. Wei, X. Cui, T. J. Lu, P. M. Belinda, F. Li, F. Xu, *Adv. Funct. Mater.* **2016**, *26*, 165.
- [37] M. Weng, P. Zhou, L. Chen, L. Zhang, W. Zhang, Z. Huang, C. Liu, S. Fan, *Adv. Funct. Mater.* **2016**, *26*, 7244.
- [38] S. Gong, W. Schwalb, Y. Wang, Y. Chen, Y. Tang, J. Si, B. Shirinzadeh, W. Cheng, *Nat. Commun.* **2014**, *5*, 3132.
- [39] X. Liu, M. Mwangi, X. Li, M. O'Brien, G. M. Whitesides, *Lab Chip* **2011**, *11*, 2189.
- [40] T. Kang, *Appl. Phys. Lett.* **2014**, *104*, 073117.
- [41] Y. L. Han, H. Liu, C. Ouyang, T. J. Lu, F. Xu, *Sci. Rep.* **2015**, *5*, 11488.
- [42] Q. Hua, H. Liu, J. Zhao, D. Peng, X. Yang, L. Gu, C. Pan, *Adv. Electron. Mater.* **2016**, *2*, 1600093.
- [43] Q. Zhong, J. Zhong, X. Cheng, X. Yao, B. Wang, W. Li, N. Wu, K. Liu, B. Hu, J. Zhou, *Adv. Mater.* **2015**, *27*, 7130.
- [44] J. Ahn, J. Seo, T.-I. Lee, D. Kwon, I. Park, T.-S. Kim, J. Lee, *ACS Appl. Mater. Interfaces* **2016**, *8*, 19031.
- [45] S. C. B. Mannsfeld, B. C.-K. Tee, R. M. Stoltenberg, C. V. H.-H. Chen, S. Barman, B. V. O. Muir, A. N. Sokolov, C. Reese, Z. Bao, *Nat. Mater.* **2010**, *9*, 859.
- [46] S. Park, H. Kim, M. Vosgueritchian, S. Cheon, H. Kim, J. H. Koo, T. R. Kim, S. Lee, G. Schwartz, H. Chang, Z. Bao, *Adv. Mater.* **2014**, *26*, 7324.
- [47] C. M. Boutry, A. Nguyen, Q. O. Lawal, A. Chortos, S. Rondeau-Gagné, Z. Bao, *Adv. Mater.* **2015**, *27*, 6954.
- [48] S. Kang, J. Lee, S. Lee, S. Kim, J. Kim, H. Algadi, S. Al-sayari, D. Kim, D. Kim, T. Lee, *Adv. Electron. Mater.* **2016**, *2*, 1600356.
- [49] S. Cho, S. Lee, S. Yu, H. Kim, S. Chang, D. Kang, I. Hwang, H. Kang, B. Jeong, E. Kim, S. Cho, K. Kim, H. Lee, W. Shim, C. Park, *ACS Appl. Mater. Interfaces* **2017**, *9*, 10128.
- [50] T. Li, H. Luo, L. Qin, X. Wang, Z. Xiong, H. Ding, Y. Gu, Z. Liu, T. Zhang, *Small* **2016**, *12*, 5042.
- [51] L. Viry, A. Levi, M. Tolaro, A. Mondini, V. Mattoli, B. Mazzolai, L. Beccai, *Adv. Mater.* **2014**, *26*, 2659.
- [52] J. N. Lee, C. Park, G. M. Whitesides, *Anal. Chem.* **2003**, *75*, 6544.
- [53] M. Abdelgawad, C. Wu, W.-Y. Chien, W. R. Geddie, M. A. S. Jewett, Y. Sun, *Lab Chip* **2011**, *11*, 545.
- [54] P. Kim, M. Abkarian, H. A. Stone, *Nat. Mater.* **2011**, *10*, 952.
- [55] B. N. J. Persson, *Surf. Sci. Rep.* **2006**, *61*, 201.
- [56] N. Özkaya, M. Nordin, D. Goldsheyder, D. Leger, *Fundamentals of Biomechanics: Equilibrium, Motion, and Deformation*, Springer, New York **2012**, Ch. 15.
- [57] R. E. Mark, C. Habeger, J. Borch, M. B. Lyne, *Handbook of Physical Testing of Paper*, Vol. 1, Marcel Dekker, New York **2001**, Ch. 3.
- [58] M. Alava, K. Niskanen, *Rep. Prog. Phys.* **2006**, *69*, 669.
- [59] H. W. Haslach, *Mech. Time-Depend. Mater.* **2000**, *4*, 169.
- [60] F. Carrillo, S. Gupta, M. Balooch, S. J. Marshall, G. W. Marshall, L. Pruitt, C. M. Puttlitz, *J. Mater. Res.* **2005**, *20*, 2820.
- [61] K. Schulgasser, *Fibre Sci. Technol.* **1981**, *15*, 257.

Received: February 2, 2017
Revised: March 31, 2017
Published online: May 19, 2017